J. Fluid Mech. (1984), *vol.* 143, *pp.* 173–195
Printed in Great Britain

Stokeslet arrays in a pipe and their application to ciliary transport

By N. LIRON

Department of Mathematics, Technion, Israel Institute of Technology, Haifa 32000, Israel

(Received 27 June 1983 and in revised form 13 February 1984)

The problem of fluid transport by cilia in a circular cylinder is investigated. The discrete-cilia approach is used in building the model, using the Green function due to an infinite periodic Stokeslet array in a pipe. Two different expressions are obtained for the Green function, one via a residue method and the other using the Poisson summation formula each amenable for computation in a different region. Interaction of the Stokeslets is investigated to see how, as distance decreases, interaction changes from initially separated closed vortices to a continuous flow. The singular integral equations for the forces in this model are now replaced by non-singular equations, thus overcoming the numerical difficulties in earlier works. It is found that in the pipe core the flow is time-independent and varies between a plug flow and a negative parabolic profile, in the pumping range. These results are seen to be local results due to the near field. Streamlines in the sublayer show eddies near the cilia bases blending into a uniform flow near the cilia tips.

1. Introduction

One of the major functions of cilia is the transport of fluid for such tasks as feeding and respiration in plants, transport of gametes in the reproductive system, or generation of feeding currents such as for *Vorticella* or other suspension feeders.

Using an envelope model, Lardner & Shack (1972) calculated flow of sperm in the ductus efferentes of the male reproductive tract and obtained results two orders of magnitude less than those observed (see Blum 1974). Recognizing the need for a more accurate description of the cilia function, Blake (1973) proposed using his cilia sublayer model for the flow due to cilia above an infinite flat plate (Blake 1972), approximating a tubule by two parallel plates taking the one-plate solution near each plate, and then connecting the two profiles by a flat or a parabolic profile.

Blake's approach had two drawbacks. The first was the inaccuracy of his cilia sublayer model, in which a cilium interacts with the mean flow instead of the instantaneous flow field it beats in. Since the forces a cilium develops are proportional to the difference in velocities between its velocity and the surrounding velocity this may cause large inaccuracies. The cilia sublayer model was extended by Liron & Mochon (1976*a*), the so-called discrete cilia approach, to include the time variations in the cilia layer and thus overcome this inaccuracy. Both these models use a distribution of Green functions due to Stokeslets along the centreline of each cilium as an approximation to the action of the cilium. Secondly, in Blake's (1973) approach the Green function used was the solution due to a Stokeslet above an infinite flat plate. Instead Liron (1978) argued that the proper Green function to use was the flow due to a Stokeslet between parallel plates, given by Liron & Mochon (1976*b*). This approach yielded a natural break-up of the flow between the plates into two

components; the flow due to Stokeslets action with zero flux and a positive pressure head, and a plane Poiseuille flow with a non-zero flux. Thus the role of the pressure was explained.

In Liron & Mochon (1976*a*) and Liron (1978) it was shown that the time-dependent and wave-dependent variations die out at a height of a few cilia lengths above the cilia layer. Thus for 'deep' channels (in which the channel width is much larger than a cilium length) the action of the cilia is like that of a boundary layer, changing the no-slip condition to a free-slip condition, a short distance away from the walls. This result was used by Blake, Liron & Aldis (1982), to show flow patterns in ciliated ducts, allowing for variability in action at different regions. This approach yields a general picture of the flow patterns, but can be compared with experiments only qualitatively. A similar crude approach was used by Liron & Meyer (1980) to explain particle flow above an active ciliated epithilium observed in experiments.

In Liron (1978) similarities were argued between flow between parallel plates and flow in a pipe. To produce a flow similar to pipe flow we had to 'break up' the infinite extent of the lateral direction (lateral to the direction of the flow). This was done by taking a periodic array of cilia in the lateral direction, and it was shown that the flow resulting would be similar in general features to flow in a pipe, provided the cilia are dense and we are modelling a wide pipe (i.e. the radius of the pipe is large compared to a cilium length). The periodic volumes compared were a wedge in a pipe with a parallelepiped in between the plates. In this paper we deal directly with transport in a pipe. This model is necessary if one is to obtain more than a qualitative result or if the ratio of cilium length to pipe radius is not large, as in the ductus efferentes. This is now possible as the solution due to a Stokeslet in an infinite pipe is now known (Liron & Shahar 1978, henceforth referred to as LS).

In Liron (1978) the so-called discrete-cilia approach was used. The same model is used in the present paper. In this model the action of each cilium is approximated by a distribution of Stokeslets along its centreline, and after suitable periodicity assumptions and metachronal coordination between the cilia an expression for the velocities is obtained. This expression depends on the unknown strengths of the Stokeslets distributed along the cilia centrelines. These are then found by giving a kinematic description of the cilia movement, yielding a singular integral equation. In similar problems (Blake 1972; Liron & Mochon 1976*a*) the singularity was essentially ignored. In Liron (1978) this problem was recognized and the action of a Stokeslet on itself was replaced by the action of the Stokeslet on a point on the cilia surface at the same cross-section. The results depended then on which point was chosen. We now render the equations non-singular by using a result due to Lighthill (1976). This enables us to obtain good accuracy. Also, this enables us to look into the cilia sublayer to observe how the flow inside the layer merges into the uniform flow it creates outside the layer.

The basic building block of the model is an infinite periodic array of Stokeslets inside an infinite straight cylinder. This Green function is of special interest in itself. Recently it has become clear that eddies are to be expected in Stokes flows (see Hasimoto & Sano 1980, and references therein). An attempt at explaining development of such eddies was made by Liron & Blake (1981). The flow due to a Stokeslet changes drastically with confinement of the flow due to boundaries. For infinite medium there are no eddies and velocities decay as r^{-1} ($r \equiv$ the distance from the force). Once the force is next to a plane boundary the decay is as r^{-2} for parallel orientation of the force and r^{-3} for vertical orientation. Also for vertical orientation a single (toroidal) eddy exists. Once two plane boundaries are present the decay rate becomes r^{-2} for

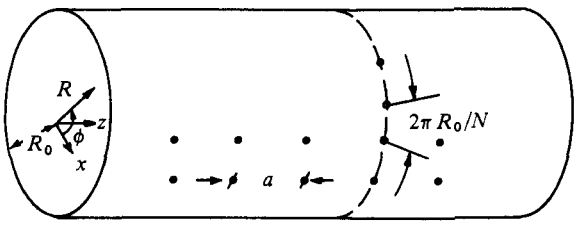

FIGURE 1. The cilia-base distribution on the surface of the pipe, cilia are evenly distributed every distance a longitudinally, and every $2\pi R_0/N$ circumferentially. Cilia beat synchronously, with no phase difference in each ring, and a phase difference down the pipe causing a metachronal wave.

a force parallel to the boundaries but with a pair of symmetric eddies (asymptotically we obtain a two-dimensional Hele Shaw doublet). For a force perpendicular to the plane boundaries an infinite set of Moffatt (1964) type eddies exist, with velocities decaying exponentially with r (measured in units of the distance between the boundaries). Inside a pipe the exponentially decaying Moffatt-type eddies exist for all force orientations (see LS; Blake 1979; Liron & Blake 1981). With the present knowledge that Stokeslets create eddies whenever boundaries or obstacles are present, and in particular inside a pipe we have an infinite series of eddies with exponentially decaying strength, the question arises as to how these Stokeslet solutions superimpose to obtain a continuous downstream flow.

In §2 we present the model used. This is essentially the model used in Liron (1978), except for the different geometry. In §3 the analytic development of the infinite-array Green function is given. Two different expressions are derived yielding theoretical insight as well as enabling us to compute the solutions easily in the entire region. Streamlines for this Green function for several cases are given in §4. The integral equations including the improvement rendering them non-singular are given in §5. Examples of numerical results due to a two-dimensional beat, including streamlines in the cilia layer, are shown in §6.

2. The cilia model

We distribute cilia uniformly on the surface of an infinite straight pipe of radius R_0 (see figure 1). Let the bases of the cilia be at

$$\left.\begin{aligned} R &= R_0, \\ z &= ma \quad (m = 0, \pm 1, \pm 2, \ldots), \\ \Phi &= \phi_j = \frac{2\pi j}{N} \quad (j = 0, \ldots, N-1), \end{aligned}\right\} \tag{2.1}$$

where (R, z, Φ) are cylindrical coordinates. Let the coordinates of the centreline of the cilium based at $(R_0, 0, 0)$ be

$$\begin{aligned} \boldsymbol{\xi}(s,t) &= (\xi_1(s,t), \xi_2(s,t), \xi_3(s,t)) \\ &= (r(s,t), Z(s,t), \phi(s,t)) \quad (0 \leqslant s \leqslant 1,\ 0 \leqslant t \leqslant T), \end{aligned} \tag{2.2}$$

where $|\boldsymbol{\xi}(1,t)| = L$, the cilium length ($< R_0$), and T is the period of the cilium beat. $r(0,t) = R_0$, i.e. we are measuring from base to tip. All other cilia centrelines will have coordinates

$$\xi'_{m,j}(s,t) = (r(s,\tau_m),\ ma + Z(s,\tau_m),\ \phi_j + \phi(s,\tau_m)), \tag{2.3}$$

where

$$\tau_m = t \pm \frac{ma\kappa}{\sigma} \quad (m = 0, \pm 1, \pm 2, \ldots), \tag{2.4}$$

representing a metachronal wave moving down the pipe. (In Liron & Mochon (1976*a*) and Liron (1978) τ_m was erroneously written as $\kappa ma \pm \sigma t$.) Assuming the effective stroke of the ciliary beat cycle to be in the positive z-direction, the metachronal wave is called symplectic if the coordination wave is propagated in the positive z-direction (i.e. minus sign in τ_m) and antiplectic when propagated in the negative z-direction (i.e. plus sign in τ_m). For this wave we have wave velocity $c = \sigma/\kappa$, wavelength $\Lambda = 2\pi/\kappa$, frequency $f = \sigma/2\pi$, period $T = 2\pi/\sigma$.

2.1. *The flow fields*

We distribute Stokeslets along the centrelines with an unknown force distribution $\boldsymbol{F} = (F_1, F_2, F_3)$ and sum over all cilia. The total velocity is thus

$$u_j(R, z, \Phi, t) = \sum_{m=-\infty}^{\infty} \sum_{n=0}^{N-1} \int_0^1 F_k(\xi'_{m,n}(s,t))\, G_j^k(R, z, \Phi, \xi'_{m,n}(s,t))\, \mathrm{d}s \quad (j = 1, 2, 3). \tag{2.5}$$

Here $G_j^k(R, z, \Phi, \xi'_{m,n})$ is the jth component of the velocity at (R, z, Φ) due to a Stokeslet at $\xi'_{m,n}$ pointing in the kth direction, $k = 1, 2, 3$, see (2.2), and the Einstein summation convention is used. G_j^k is given in Liron & Shahar (1978). The following assumptions are now made.

Assumption I. The velocity is periodic in Φ with a period of $2\pi/N$:

$$u_j(R, z, \Phi, t) = u_j(R, z, \Phi + 2\pi/N, t). \tag{2.6}$$

From (2.6) it follows that

$$\boldsymbol{F}(\xi'_{m,n}(s,t)) = \boldsymbol{F}(\xi'_{m,0}(s,t)) \tag{2.7}$$

for all n. To obtain (2.7) we have

$$u_j = \sum_{m=-\infty}^{\infty} \sum_{n=0}^{N-1} \int_0^1 F_k(\xi'_{m,n}(s,t))\, G_j^k(R, z, \Phi + 2\pi/N, \xi'_{m,n}(s,t))\, \mathrm{d}s,$$

from (2.5) and (2.6). Since G_j^k depends on Φ and $\phi_j + \phi$ only through their difference (Liron & Shahar 1978), it follows that

$$u_j = \sum_{m=-\infty}^{\infty} \sum_{n=0}^{N-1} \int_0^1 F_k(\xi'_{m,n}(s,t))\, G_j^k(R, z, \Phi, \xi'_{m,n-1})\, \mathrm{d}s,$$

where $\xi'_{m,-1} \equiv \xi'_{m,N-1}$. If there is a unique force distribution for a given velocity field, i.e. $\boldsymbol{F} \equiv 0$ if $\boldsymbol{u} \equiv 0$, then comparing the last line with (2.5) we obtain

$$F(\xi'_{m,n+1}) = F(\xi'_{m,n}) \quad (n = 0, \ldots, N-1),$$

from which (2.7) follows.

Assumption II. The velocity is periodic in z with a period a, *but* with a time difference at Δt, the time it takes the wave to travel the distance a:

$$u_j(R, z, \Phi, t) = u_j(R, z \pm a, \Phi, t - \Delta t), \tag{2.8}$$

$$\Delta t = a\kappa/\sigma. \tag{2.9}$$

The $\pm$ signs in (2.8) have the same meaning as in (2.4). It follows that

$$\boldsymbol{F}(\xi'_{m,0}(s,t)) = \boldsymbol{F}(\xi(s, \tau_m)). \tag{2.10}$$

The proof is identical with that given in Liron & Mochon (1976*a*), and will not be repeated here. Using (2.7) and (2.10), we may now rewrite (2.5) as

$$u_j(R,z,\Phi,t) = \sum_{m=-\infty}^{\infty} \sum_{n=0}^{N-1} \int_0^1 F_k(\xi(s,\tau_m))\, G_j^k(R,z,\Phi,\xi'_{m,n}(s,t))\,\mathrm{d}s. \tag{2.11}$$

Assumption III. The cilia pattern has the same wavelength as the metachronal wave. If we have m_0 different cilia positions in one wavelength then

$$\Lambda = m_0 a \quad (\kappa = 2\pi/m_0 a). \tag{2.12}$$

This assumption is a simplification enabling us to take advantage of the periodicity.

We shall make one more important simplification. Since cilia are dense ($N \gg 1$) and the flow is periodic in Φ with period $2\pi/N$, it is almost uniform in Φ, so we average on Φ over one period:

$$\bar{u}_j(R,z,t) = \frac{1}{(2\pi/N)\,R} \int_0^{2\pi/N} R u_j(R,z,\Phi,t)\,\mathrm{d}\Phi. \tag{2.13}$$

If we denote the axisymmetric part of G_j^k by v_j^k, we obtain, from (2.11) and (2.13),

$$\bar{u}_j(R,z,t) = N \sum_{m=-\infty}^{\infty} \int_0^1 F_k(\xi(s,\tau_m))\, v_j^k(R,z,\xi'_m(s,t))\,\mathrm{d}s, \tag{2.14}$$

where

$$\xi'_m(s,t) = (r(s,\tau_m), ma + Z(s,\tau_m), 0). \tag{2.15}$$

Using the relation (2.12) for the wavelength, we can transform (2.14) in a manner similar to that in Liron & Mochon (1976*a*) or Liron (1978), to obtain

$$\bar{u}_j(R,z,t) = N \sum_{l=0}^{m_0-1} \int_0^1 F_k(\xi^l(s,t))\, D_j^k(R,z-la,\xi^l(s,t))\,\mathrm{d}s, \tag{2.16}$$

where

$$\xi^l(s,t) = \xi(s,\tau_l), \tag{2.17}$$

and

$$D_j^k(R,z,\xi) = \sum_{m=-\infty}^{\infty} v_j^k(R,z+m\Lambda,\xi). \tag{2.18}$$

The kernel D_j^k is our basic building block, and represents the sum of an infinite sequence of Stokeslet rings of radius R situated inside the pipe at $\xi + m\Lambda$ ($m = 0, \pm 1, \pm 2, \ldots$). This kernel is discussed in the following sections. As already seen in Liron (1978), we can add in general a Poiseuille flow. This is

$$v_j(R) = -\frac{1}{4\mu}\frac{\partial p}{\partial z}(R_0^2 - R^2)\,\delta_{j2}, \tag{2.19}$$

where the pressure gradient $\partial p/\partial z$ is constant. The total velocity is thus

$$U_j(R,z,t) = \bar{u}_j(R,z,t) + v_j(R). \tag{2.20}$$

2.2. *Pressure gradient and flux*

Associated with $\bar{u}_j$ we also obtain a pressure head in the z-direction. The pressure gradient can be simplified in a manner similar to the velocity, and is found to be

$$\frac{\partial P}{\partial z} = N \sum_{l=0}^{m_0-1} \int_0^1 F_k(\xi^l(s,t)) \frac{\partial \bar{P}^k}{\partial z}(R,z-la,\xi^l(s,t))\,\mathrm{d}s. \tag{2.21}$$

The kernel $\partial \bar{P}^k/\partial z$ is also given in §3.

The pressure head ΔP per wavelength in the z-direction is obtained from (2.19) and (2.21) and found to be

$$\Delta P = \Lambda\left\{\frac{\partial p}{\partial z} + N\sum_{l=0}^{m_0-1}\int_0^1 F_2(\xi^l(s,t))\frac{\kappa}{\pi^2 R_0^2}\left[1-\left(\frac{\xi_1^l(s,t)}{R_0}\right)^2\right]\mathrm{d}s\right\}. \tag{2.22}$$

The flux due to $\bar{u}_j$ is zero (see Liron 1978), and thus the total flux Q is given by

$$Q = \int_{R=0}^{R_0}\int_{\phi=0}^{2\pi} Rv_2(R)\,\mathrm{d}R\,\mathrm{d}\phi = \frac{\pi}{8\mu}\left(-\frac{\partial p}{\partial z}\right)R_0^4. \tag{2.23}$$

We shall be interested in cilia performance in the pumping range ($\Delta P \geqslant 0$, $Q \geqslant 0$) so we demand $-\partial p/\partial z \geqslant 0$, i.e. the added Poiseuille flow is flowing in the positive z-direction. In this case the maximum pressure head will exist when $Q = 0$ (obviously for $Q < 0$, ΔP will be larger). As we shall see below in §6, this does not mean that one actually sees a downstream Poiseuille flow. Quite to the contrary, one sees an upstream Poiseuille flow almost everywhere. But the pumping range is the region where cilia action fall under the definition of a pump. Results for other cases are clear from the numerical results and the structure of the separate flow fields in (2.20).

3. The Stokeslet arrays

As seen in §2, our basic building block is the kernel $D_j^k(b,z,\boldsymbol{\xi})$ and represents the sum of an infinite array of uniform Stokeslet rings of radius bR_0 ($< R_0$), where R_0 is the radius of the pipe. The Stokeslet rings are distributed longitudinally (down the pipe) with distance ΛR_0.

In LS the general solution due to a single Stokeslet in an infinite pipe was given. We thus have to take the component multiplying $\cos(0)$ and sum an infinite series of these a distance ΛR_0 apart downstream to obtain D_j^k. This can be done in two ways, corresponding to the two forms of the solution shown in LS, the integral form and the residue form, both of them necessary for computational purposes.

3.1. *The integral form*

We shall demonstrate derivation of the result for D_z^z. In LS we had, for $V_z^z = (u_0)_z^z$ due to a single Stokeslet,

$$V_z^z(R,z,b) = V_z^z = g_z^z + v_z^z, \tag{3.1}$$

where g_z^z, v_z^z may be computed by the formulae in LS. These are

$$(-4\pi^2 R_0)\,g_z^z = \int_0^\infty \frac{\cos\lambda z}{\Delta_0(\lambda)}G(\lambda,R,b)\,\mathrm{d}\lambda, \tag{3.2}$$

where

$$\Delta_0(\lambda) = \lambda[I_0^2(\lambda) - I_1^2(\lambda)] - 2I_1(\lambda)\,I_0(\lambda), \tag{3.3}$$

$$G(\lambda,R,b) = \lambda I_0(\lambda R)\,[(2A(\lambda)-1)\,I_0(\lambda b) + \lambda b A(\lambda)\,I_1(\lambda b)] + \lambda R I_1(\lambda R)\,[\lambda A(\lambda)\,I_0(\lambda b) - bI_1(\lambda b)], \tag{3.4}$$

$$A(\lambda) = K_0(\lambda)\,I_2(\lambda) + K_1(\lambda)\,I_1(\lambda). \tag{3.5}$$

Here and henceforth all lengths are non-dimensionalized with respect to R_0.

For v_z^z we have

$$4\pi^2\mu R_0 v_z^z = \int_0^\infty \mathrm{d}\lambda \cos\lambda z[I_0(\lambda b)(2K_0(\lambda R)-\lambda R K_1(\lambda R))+\lambda b I_1(\lambda b) K_0(\lambda R)] \quad (R > b); \tag{3.6}$$

for $R < b$ we interchange R and b in (3.6).

We first extend the integrals in (3.2) and (3.6) to the interval $(-\infty, \infty)$. Since the functions K_0 and K_1 have a cut along the negative real axis, and both contain a logarithm (see Abramowitz & Stegun 1965), we transfer (3.2) by $s = \lambda \exp(\mathrm{i}\pi)$ to

$$-4\pi^2\mu g_z^z = \int_{-\infty}^0 \frac{\cos sz}{\Delta_0(s)} G(s, R, b)\,\mathrm{d}s - \pi\mathrm{i}\int_{-\infty}^0 H(s, R, b)\cos sz\,\mathrm{d}s,$$

where

$$H(s, R, b) = I_0(sR)(2I_0(sb)+sbI_1(sb))+sRI_1(sR)I_0(sb).$$

Thus

$$-8\pi^2\mu g_z^z \equiv \int_{-\infty}^\infty \frac{\cos\lambda z}{\Delta_0(\lambda)} G(\lambda, R, b)\,\mathrm{d}\lambda - \pi\mathrm{i}\int_{-\infty}^0 H(\lambda, R, b)\cos\lambda z\,\mathrm{d}\lambda.$$

Similarly for v_z^z we obtain

$$8\pi^2\mu R_0 v_z^z = \int_{-\infty}^\infty \mathrm{d}\lambda \cos\lambda z\,[I_0(\lambda b)(2K_0(\lambda R)-\lambda R K_1(\lambda R)) + \lambda b I_1(\lambda b) K_0(\lambda R)] - \pi\mathrm{i}\int_{-\infty}^0 H(\lambda, R, b)\cos\lambda z\,\mathrm{d}\lambda.$$

Thus the sum of the two cancels the integral that multiplies $\pi\mathrm{i}$ (which is divergent, and strictly speaking we should have dealt with the sum and not each component separately). Thus we obtain

$$8\pi^2\mu R_0 V_z^z = -\int_{-\infty}^\infty \frac{\cos\lambda z}{\Delta_0(\lambda)} G(\lambda, R, b)\,\mathrm{d}\lambda + \int_{-\infty}^\infty [I_0(\lambda b)(2K_0(\lambda R)-\lambda R K_1(\lambda R)) + \lambda b I_1(\lambda b) K_0(\lambda R)]\cos\lambda z\,\mathrm{d}\lambda \quad (R > b); \tag{3.7}$$

for $R < b$ we interchange R and b in the second integral of (3.7). The integrand in (3.7) is now even. Thus we may write (3.7) as

$$8\pi^2\mu R_0 V_z^z = \int_{-\infty}^\infty \cos\lambda z f(\lambda, R, b)\,\mathrm{d}\lambda = \int_{-\infty}^\infty \mathrm{e}^{\mathrm{i}\lambda z} f(\lambda, R, b)\,\mathrm{d}\lambda.$$

For D_z^z we obtain an equation of the form

$$\begin{aligned} D_z^z &= \sum_{m=-\infty}^{\infty} \int_{-\infty}^\infty \mathrm{e}^{\mathrm{i}\lambda(z-m\Lambda)} f(\lambda, R, b)\,\mathrm{d}\lambda = \sum_{m=-\infty}^{\infty} \int_{-\infty}^\infty \mathrm{e}^{-m(\lambda/\kappa)2\pi\mathrm{i}}\,\mathrm{e}^{\mathrm{i}\lambda z} f\,\mathrm{d}\lambda \\ &= \sum_{m=-\infty}^{\infty} \int_{-\infty}^\infty \cos\lambda z\,\mathrm{e}^{-2\pi\mathrm{i}(\lambda/\kappa)m} f(\lambda, R, b)\,\mathrm{d}\lambda \\ &= \kappa \sum_{m=-\infty}^{\infty} \cos m\kappa z f(\kappa m, R, b), \end{aligned} \tag{3.8}$$

where

$$\kappa = 2\pi/\Lambda, \tag{3.9}$$

and we have used the Poisson summation formula in the last step.

In this manner we obtain the following expressions for D_j^k (all equations should be multiplied by a unit force per volume):

$$D_R^z = \frac{\kappa}{4\pi^2\mu R_0}\Bigg\{\sum_{\substack{m=1\\ \lambda=\kappa m}}^{\infty} \sin\lambda z[\lambda R K_0(\lambda R)\, I_0(\lambda b) - \lambda b K_1(\lambda R)\, I_1(\lambda b)]$$

$$+ \sum_{\substack{m=1\\ \lambda=\kappa m}}^{\infty} \frac{\sin\lambda z}{\Delta(\lambda)}[bRI_1(\lambda b)\, I_2(\lambda R) + I_1(\lambda R)\,(I_0(\lambda b) - \lambda b I_1(\lambda b)\, A(\lambda))$$

$$-\lambda R I_0(\lambda R)\, I_0(\lambda b)\, A(\lambda)]\Bigg\} \quad (R > b); \tag{3.10}$$

for $R < b$ we interchange the brackets in the first sum by

$$[\lambda R K_0(\lambda b)\, I_0(\lambda R) - \lambda b K_1(\lambda b)\, I_1(\lambda R)]; \tag{3.11}$$

$A(\lambda)$ is given in (3.5) and

$$\Delta(\lambda) = I_0(\lambda)\, I_2(\lambda) - I_1^2(\lambda), \tag{3.12}$$

$$D_\phi^z = 0; \tag{3.13}$$

$$D_z^z = \frac{\kappa}{4\pi^2\mu R_0}\Bigg\{-(1-b^2)(1-R^2) + \ln\frac{1}{b}$$

$$+ \sum_{\substack{m=1\\ \lambda=\kappa m}}^{\infty} [K_0(\lambda b)\,(2I_0(\lambda R) + \lambda R I_1(\lambda R)) - \lambda b K_1(\lambda b)\, I_0(\lambda R)]\cos\lambda z$$

$$+ \sum_{\substack{m=1\\ \lambda=\kappa m}}^{\infty} [bRI_1(\lambda b)\, I_1(\lambda R) + I_0(\lambda R)\, I_0(\lambda b) - A(\lambda)\,(\lambda b I_0(\lambda R)\, I_1(\lambda b)$$

$$+\lambda R I_1(\lambda R)\, I_0(\lambda b) + 2I_0(\lambda R)\, I_0(\lambda b))]\frac{\cos\lambda z}{\Delta(\lambda)}\Bigg\} \quad (R < b); \tag{3.14}$$

for $R > b$ we interchange R and b in (3.14).

For the pressure gradient we obtain

$$\frac{\partial P^z}{\partial z} = \frac{\kappa}{2\pi^2 R_0^3}\Bigg\{2(1-b^2) + \sum_{\substack{m=1\\ \lambda=\kappa m}}^{\infty} \lambda^2 I_0(\lambda R)\, K_0(\lambda b)\cos\lambda z$$

$$- \sum_{\substack{m=1\\ \lambda=\kappa m}}^{\infty} [\lambda^2 I_0(\lambda b)\, A(\lambda) - \lambda b I_1(\lambda b)]\, I_0(\lambda R)\frac{\cos\lambda z}{\Delta(\lambda)}\Bigg\} \quad (R < b); \tag{3.15}$$

for $R > b$ we interchange R and b in the first sum of (3.15) only.

Equations (3.10)–(3.15) give the solution due to a line of Stokeslets in the z-direction. The z-independent components of (3.14) and (3.15) are the components left by averaging over one 'wavelength' Λ in the z-direction. These are

$$\overline{D}_z^z = \frac{\kappa}{4\pi^2\mu R_0}\begin{cases}\ln(1/b) - (1-b^2)(1-R^2) & (R < b),\\ \ln(1/R) - (1-b^2)(1-R^2) & (R > b),\end{cases} \tag{3.16}$$

$$\frac{\partial \overline{P}^z}{\partial z} = \frac{\kappa}{\pi^2 R_0^3}(1-b^2), \tag{3.17}$$

and have the following interpretation. $\overline{D}_z^z$ corresponds to a flow field due to a cylinder of radius b concentric to the pipe (radius 1) and moving with velocity $(\kappa/4\pi^2\mu R_0)\ln(1/b)$

parallel to itself in the z-direction. Such a flow consists of a uniform motion inside ($R < b$) and a shear flow $-\ln R$ to the outer stationary wall. No pressure head is associated with this flow. This flow creates a non-zero flux. To compensate to zero flux one adds a Poiseuille flow $-(1-b^2)(1-R^2)$ in the direction of $-z$, which is the second part of $\bar{D}_z^z$. This has the associated (positive) pressure gradient as in (3.17). Indeed, the flux due to the shearing cylinder is

$$Q_1 = \frac{\kappa}{4\pi^2\mu R_0}\left[\int_0^b R\ln\frac{1}{b}\,\mathrm{d}R + \int_b^1 R\ln\frac{1}{R}\,\mathrm{d}R\right] = \tfrac{1}{4}(1-b^2)\frac{\kappa}{4\pi^2\mu R_0},$$

and the flux due to the negative Poiseuille flow

$$Q_2 = \frac{-\kappa(1-b^2)}{4\pi^2\mu R_0}\int_0^1 R(1-R^2)\,\mathrm{d}R = -Q_1. \tag{3.18}$$

For Stokeslets in the radial direction one obtains

$$\begin{aligned} D_R^R = \frac{\kappa}{4\pi^2\mu R_0}\Bigg\{ & \sum_{\substack{m=1\\ \lambda=\kappa m}}^{\infty} [\lambda R K_0(\lambda R)\, I_1(\lambda b) - \lambda b K_1(\lambda R)\, I_2(\lambda b)]\cos\lambda z \\ & + \sum_{\substack{m=1\\ \lambda=\kappa m}}^{\infty} \frac{\cos\lambda z}{\Delta(\lambda)}\Bigg[R I_0(\lambda R)\left(b I_0(\lambda b) - \left(\frac{2}{\lambda}+\lambda A(\lambda)\right) I_1(\lambda b)\right) \\ & + I_1(\lambda R)\left(I_1(\lambda b) - b\left(\frac{2}{\lambda}+\lambda A(\lambda)\right) I_2(\lambda b)\right)\Bigg]\Bigg\} \quad (R > b); \end{aligned} \tag{3.19}$$

for $R < b$ we interchange R and b in (3.19).

$$D_\phi^R = 0, \tag{3.20}$$

$$\begin{aligned} D_z^R = \frac{\kappa}{4\pi^2\mu R_0}\Bigg\{ & \sum_{\substack{m=1\\ \lambda=\kappa m}}^{\infty} [\lambda R K_1(\lambda R)\, I_1(\lambda b) - \lambda b K_0(\lambda R)\, I_0(\lambda b)]\sin\lambda z \\ & + \sum_{\substack{m=1\\ \lambda=\kappa m}}^{\infty}\Bigg[I_0(\lambda R)\,(\lambda b I_0(\lambda b)\, A(\lambda) - I_1(\lambda b)) \\ & + R I_1(\lambda R)\left(\left(\frac{2}{\lambda}+\lambda A(\lambda)\right) I_1(\lambda b) - b I_0(\lambda b)\right)\Bigg]\frac{\sin\lambda z}{\Delta(\lambda)}\Bigg\} \quad (R > b). \end{aligned} \tag{3.21}$$

for $R < b$ we replace the square brackets in the first sum in (3.21) by

$$[\lambda R I_1(\lambda R)\, K_1(\lambda b) - \lambda b K_0(\lambda b)\, I_0(\lambda R)]. \tag{3.22}$$

For the pressure we obtain

$$\begin{aligned} P^R = \frac{\kappa}{2\pi^2 R_0^2}\Bigg(& b(1-\tfrac{1}{2}b^2) + \sum_{\substack{m=1\\ \lambda=\kappa m}}^{\infty} \lambda\cos\lambda z K_0(\lambda R)\, I_1(\lambda b) \\ & + \sum_{\substack{m=1\\ \lambda=\kappa m}}^{\infty}\left[b I_0(\lambda b) - \left(\frac{2}{\lambda}+\lambda A(\lambda)\right) I_1(\lambda b)\right] I_0(\lambda R)\frac{\cos\lambda z}{\Delta(\lambda)} \quad (R > b); \end{aligned} \tag{3.23}$$

for $R < b$ we replace the entire first row in (3.23) by

$$b(1-\tfrac{1}{2}b^2) - \frac{1}{2b} - \sum_{\substack{m=1\\ \lambda=\kappa m}}^{\infty} \lambda I_0(\lambda R)\, K_1(\lambda b)\cos\lambda z. \tag{3.24}$$

As before, the components independent of z in (3.19)–(3.24) are the average over z. These are

$$\bar{D}_R^R = 0,$$

$$\bar{P}^R = \frac{\kappa}{2\pi^2 R_0^2} \begin{cases} b(1-\frac{1}{2}b^2) - \dfrac{1}{2b} & (R < b), \\ b(1-\frac{1}{2}b^2) & (R > b). \end{cases}$$

This corresponds to the situation of a cylinder of radius b pushing out radially and uniformly. By incompressibility, no flow can result, but there will be a jump in pressure as we go through $R = b$. This pressure jump is $(\kappa/2\pi^2 R_0^2)\ (1/2b)$.

For Stokeslets pointing circumferentially, we obtain

$$D_R^\phi = D_z^\phi = P^\phi = 0, \tag{3.25}$$

$$D_\phi^\phi = \frac{\kappa}{4\pi^2 \mu R_0} \left\{ \tfrac{1}{2}b\left(\frac{1}{R} - R\right) + 2 \sum_{\substack{m=1 \\ \lambda = \kappa m}}^{\infty} \cos \lambda z \frac{I_1(\lambda b)}{I_1(\lambda)} [K_1(\lambda r)\, I_1(\lambda) - K_1(\lambda)\, I_1(\lambda R)] \right\} \quad (R > b); \tag{3.26}$$

for $R < b$ we interchange R and b in (3.26). The z-independent components are now

$$\bar{D}_\phi^\phi = \frac{\kappa}{4\pi^2 \mu R_0} \begin{cases} \tfrac{1}{2}R\left(\dfrac{1}{b} - b\right) & (R < b), \\ \tfrac{1}{2}b\left(\dfrac{1}{R} - R\right) & (R > b), \end{cases}$$

$$\bar{P}^\phi = 0. \tag{3.27}$$

This flow corresponds to a cylinder of radius b rotating around its axis with velocity $(\kappa/4\pi^2 \mu R_0)\tfrac{1}{2}(1-b^2)$. This causes solid rotation inside $(R < b)$ and a rotational shear flow between this cylinder and the fixed cylinder at $R = 1$ $(R > b)$ (Couette flow). Both these flows do not have a pressure gradient associated with them.

Computation of D_j^k using (3.10) and onwards causes problems near the line $R = b$. If $R \neq b$ the asymptotic natures of the Bessel functions K (exponential decay) and I (exponential growth) ensure exponential decay of terms in both sums contributing to D_R^z (say), (3.10). But for $R = b$ the first sum does not have exponentially decaying terms, and the series converges very slowly, in particular for small κ. Thus a second form for D_j^k is needed.

3.2. *The residue form*

The velocity components by the residue technique are given in Appendix B of LS. We have to take the component $k = 0$ in (B 3) there. For example, for V_z^z we obtain, after some manipulations,

$$V_z^z = \frac{1}{4\pi\mu R_0} \operatorname{Re}\left\{ \sum_{n=1}^{\infty} \frac{d_n\, \mathrm{e}^{-d_n z}}{J_0^2(d_n)\, J_1^2(d_n)} G_z^z(b, R) \right\} \quad (z \geqslant 0), \tag{3.28}$$

where

$$G_z^z(b, R) = B_1(b)\, B_1(R), \tag{3.29}$$

$$B_1(s) = sJ_0(d_n)\, J_1(d_n s) - J_1(d_n)\, J_0(d_n s), \tag{3.30}$$

and d_n are the roots in the first quadrant of the transcendental equation

$$\alpha[J_0^2(\alpha)+J_1^2(\alpha)]-2J_0(\alpha)\,J_1(\alpha)=0. \tag{3.31}$$

A list of these roots can be found, for example, in Friedmann, Gillis & Liron (1968). The roots have an asymptotic behaviour of

$$d_n \sim (n+\tfrac{1}{2})\pi+\tfrac{1}{2}\mathrm{i}\ln((2n+1)\pi) \quad (n=0,1,2,\ldots). \tag{3.32}$$

To compute D_z^z we have to sum over all Stokeslets at $z=m\Lambda$ $(m=0,\pm1,\pm2,\ldots)$. Since for $z<0$ we have $V_z^z(z)=V_z^z(-z)$, we obtain for $0\leqslant z\leqslant\Lambda$ the sum

$$\sum_{m=0}^{\infty}\mathrm{e}^{-d_n(z+m\Lambda)}+\sum_{m=1}^{\infty}\mathrm{e}^{-d_n(m\Lambda-z)}=\frac{\cosh d_n(\frac{1}{2}\Lambda-z)}{\sinh\frac{1}{2}d_n\Lambda}. \tag{3.33}$$

Thus

$$D_z^z=\frac{1}{4\pi\mu R_0}\mathrm{Re}\left\{\sum_{n=1}^{\infty}\frac{d_n}{J_0^2(d_n)\,J_1^2(d_n)}\frac{\cosh d_n(\frac{1}{2}\Lambda-z)}{\sinh\frac{1}{2}d_n\Lambda}G_z^z(R,b)\right\} \quad (0\leqslant z\leqslant\Lambda). \tag{3.34}$$

and D_z^z is periodic in z with period Λ.

For those components in which the integral form had $\sin\lambda z$ dependence, we have $u_j^k(z)=-u_j^k(-z)$ for z negative, and the corresponding sum in (3.33) becomes

$$\sum_{m=0}^{\infty}\mathrm{e}^{-d_n(z+m\Lambda)}-\sum_{m=1}^{\infty}\mathrm{e}^{-d_n(m\Lambda-z)}=\frac{\sinh d_n(\frac{1}{2}\Lambda-z)}{\sinh\frac{1}{2}d_n\Lambda}. \tag{3.35}$$

Let

$$B_2(s)=J_0(d_n)\,J_1(d_n\,s)-sJ_1(d_n)\,J_0(d_n\,s); \tag{3.36}$$

we then obtain

$$D_R^z=\frac{1}{4\pi\mu R_0}\mathrm{Re}\left\{\sum_{n=1}^{\infty}\frac{d_n}{J_0(d_n)\,J_1^3(d_n)}\frac{\sinh d_n(\frac{1}{2}\Lambda-z)}{\sinh\frac{1}{2}d_n\Lambda}G_R^z(R,b)\right\} \quad (0\leqslant z\leqslant\Lambda), \tag{3.37}$$

with

$$G_R^z(R,b)=B_1(b)\,B_2(R), \tag{3.38}$$

and D_R^z is periodic in z with period Λ.

For the pressure gradient we obtain

$$\frac{\partial P^z}{\partial z}=\frac{1}{4\pi R_0^3}\mathrm{Re}\left\{\sum_{n=1}^{\infty}\frac{2d_n^2}{J_0(d_n)\,J_1^2(d_n)}\frac{\cosh d_n(\frac{1}{2}\Lambda-z)}{\sinh\frac{1}{2}d_n\Lambda}B_1(b)\,J_0(d_n\,R)\right\} \quad (0\leqslant z\leqslant\Lambda), \tag{3.39}$$

and periodicity in z.

Likewise we obtain

$$D_R^R=\frac{-1}{4\pi\mu R_0}\mathrm{Re}\left\{\sum_{n=1}^{\infty}\frac{d_n}{J_1^4(d_n)}\frac{\cosh d_n(\frac{1}{2}\Lambda-z)}{\sinh d_n\Lambda}B_2(b)\,B_2(R)\right\} \quad (0\leqslant z\leqslant\Lambda), \tag{3.40}$$

$$D_z^R=\frac{-1}{4\pi\mu R_0}\mathrm{Re}\left\{\sum_{n=1}^{\infty}\frac{d_n}{J_0(d_n)\,J_1^3(d_n)}\frac{\sinh d_n(\frac{1}{2}\Lambda-z)}{\sinh\frac{1}{2}d_n\Lambda}B_2(b)\,B_1(R)\right\} \quad (0\leqslant z\leqslant\Lambda), \tag{3.41}$$

and periodicity in z, with period Λ.

For the ϕ-direction we obtain

$$D_\phi^\phi=-\frac{1}{4\pi R_0}\sum_{n=1}^{\infty}\frac{\cosh c_n(z-\frac{1}{2}\Lambda)}{\sinh\frac{1}{2}c_n\Lambda}\frac{Y_1(c_n)}{J_0(c_n)}J_1(c_n\,b)\,J_1(c_n\,R) \quad (0\leqslant z\leqslant\Lambda), \tag{3.42}$$

where $c_n > 0$ and satisfy

$$J_1(c_n) = 0 \quad (n = 1, 2, \ldots). \tag{3.43}$$

From the asymptotic expression for d_n (see (3.32)) it follows that the terms in the series (3.34) and onwards decay exponentially, as long as $z \neq 0$, Λ, independent of R and b. Thus these series may be used for $R \approx b$ where the expressions in the integral form are slowly converging. If we are looking at $R \approx b$ and $z \approx 0$, both series are slowly converging, but then we are near a Stokeslet and both series should diverge in the limit $z \to 0$, $R \to b$.

The pressure head per wavelength in the case of the Stokeslets in the z-direction is obtained by integrating (3.15) over Λ. This is equivalent to integrating (3.17), and we obtain

$$\Delta P = \frac{2}{\pi R_0^2}(1 - b^2). \tag{3.44}$$

This pressure head is the same as created by a single Stokeslet from $-\infty$ to $+\infty$. A similar result was obtained for Stokeslet lines between parallel plates by Liron (1978). In a periodic flow the pressure head per wavelength is independent of the point on the cross-section where it is measured, i.e. independent of R and ϕ. Thus (3.44) is the pressure head of the flow due to a discrete array of uniform Stokeslets, as well as the pressure head due to a series of rings.

4. Flow fields due to the Stokeslet arrays

Since the flows we are dealing with are axisymmetric we can define a stream function $\psi(R, z, b)$ via

$$D_z = \frac{1}{R}\psi_R, \quad D_R = -\frac{1}{R}\psi_z \tag{4.1}$$

Using (3.10), (3.11) and (3.14), one obtains

$$\psi^z = \frac{\kappa R_0}{4\pi^2\mu}\Big\{R \sum_{\substack{m=1 \\ \lambda = \kappa m}}^{\infty} \frac{\cos \lambda z}{\lambda} f_1(\lambda, b, R) + R \sum_{\substack{m=1 \\ \lambda = \kappa m}}^{\infty} \frac{\cos \lambda z}{\lambda \Delta(\lambda)} [bRI_1(\lambda b) I_2(\lambda R) + I_1(\lambda R) I_0(\lambda b) - \lambda A(\lambda)(bI_1(\lambda b) I_1(\lambda R) + RI_0(\lambda R) I_0(\lambda b))]\Big\} + f(R, b), \tag{4.2}$$

where

$$f(R, b) = \begin{cases} -\frac{1}{4}R^2(1-b^2)(2-R^2) - \frac{1}{2}R^2 \ln b & (R < b), \\ -\frac{1}{4}R^2(1-b^2)(2-R^2) - \frac{1}{2}R^2 \ln R + \frac{1}{4}(R^2 - b^2) & (R > b), \end{cases} \tag{4.3}$$

and

$$f_1(\lambda, b, R) = \begin{cases} \lambda R K_0(\lambda b) I_0(\lambda R) - \lambda b K_1(\lambda b) I_1(\lambda R) & (R < b), \\ \lambda R K_0(\lambda R) I_0(\lambda b) - \lambda b K_1(\lambda R) I_1(\lambda b) & (R > b). \end{cases} \tag{4.4}$$

In the residue form we obtain

$$\psi^z = \frac{R_0}{4\pi\mu} \operatorname{Re}\Big\{ \sum_{n=1}^{\infty} \frac{1}{J_0(d_n) J_1^3(d_n)} \frac{\cosh d_n(\frac{1}{2}\Lambda - z)}{\sinh \frac{1}{2} d_n \Lambda} B_1(b) B_2(R) R\Big\}, \tag{4.5}$$

where B_1 and B_2 are defined in (3.30) and (3.36).

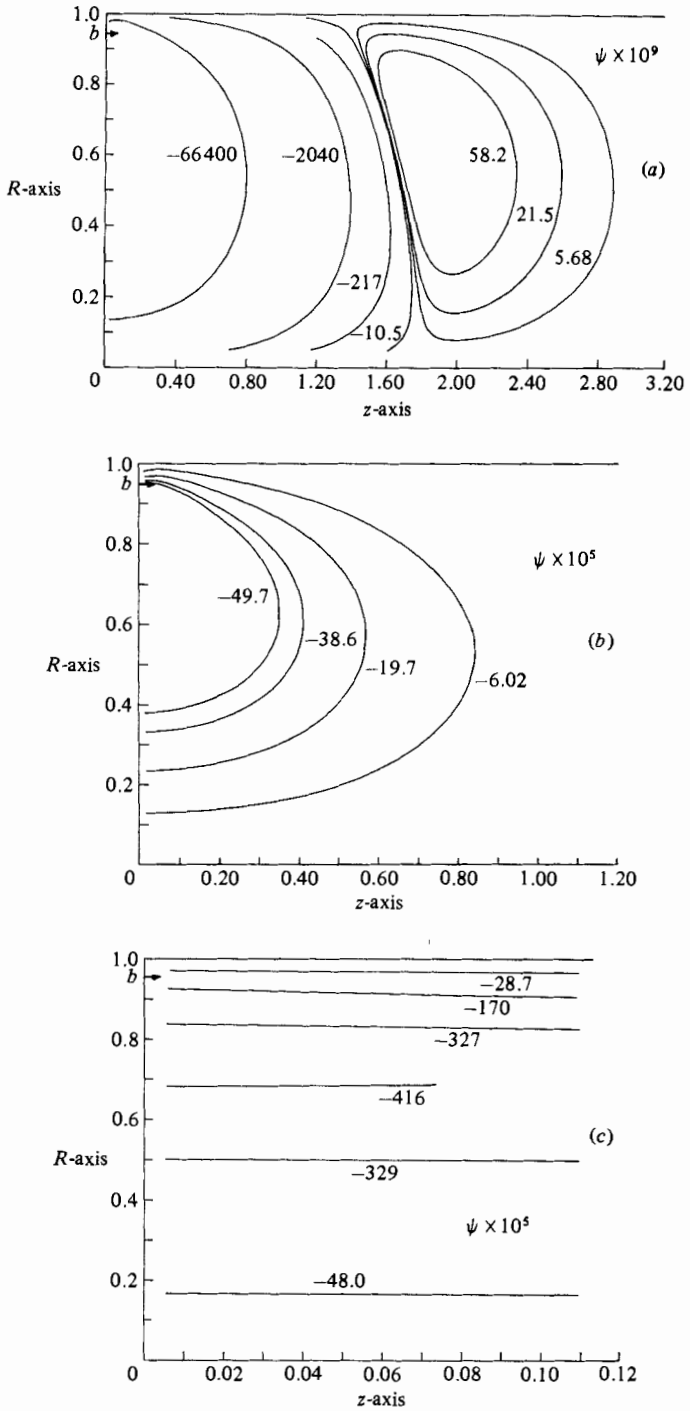

FIGURE 2. Streamlines for Stokeslets in the z-direction (see (4.2) and (4.5)) situated at a radius $b = 0.95R_0$, for: (*a*) $\kappa = 0.3$; (*b*) 3; (*c*) 30. $\kappa = 2\pi/\Lambda$ is the wavenumber of the axial array of Stokeslets. The flow field is symmetric around $z = 0$ and $z = \frac{1}{2}\Lambda$, and only the range $0 < z < \frac{1}{2}\Lambda$ is shown.

Similarly, we obtain

$$\psi^R = \frac{\kappa R_0}{4\pi^2\mu} R\Bigg\{ \sum_{\substack{m=1 \\ \lambda=\kappa m}}^{\infty} [bK_1(\lambda R)\, I_2(\lambda b) - RK_0(\lambda R)\, I_1(\lambda b)] \sin \lambda z$$

$$- \sum_{\substack{m=1 \\ \lambda=\kappa m}}^{\infty} \frac{\sin \lambda z}{\lambda \Delta(\lambda)} \Big[Rb\, I_0(\lambda R)\, I_0(\lambda b) + I_1(\lambda R)\, I_1(\lambda b)$$

$$- \Big(\frac{2}{\lambda} + \lambda A(\lambda)\Big)(RI_0(\lambda R)\, I_1(\lambda b) + bI_1(\lambda R)\, I_2(\lambda b))\Big]\Bigg\} \quad (R > b); \tag{4.6}$$

for $R < b$ we interchange R and b in the curly brackets. In the residue form

$$\psi^R = \frac{R_0}{4\pi\mu} \mathrm{Re}\Bigg\{ -R \sum_{n=1}^{\infty} \frac{1}{J_1^4(d_n)} \frac{\sinh d_n(\frac{1}{2}\Lambda - z)}{\sinh \frac{1}{2} d_n \Lambda} B_2(R)\, B_2(b) \Bigg\} \quad (0 \leqslant z \leqslant \Lambda), \tag{4.7}$$

and ψ^R is periodic in Λ. (Again notice that we have to multiply by a unit force per volume to obtain the proper dimensions.)

In the following figures we shall depict the functions $(\mu/R_0)\psi^R$ and $(\mu/R_0)\psi^z$ for various Λ and b. One of our goals is to see how the single Stokeslet, creating a series of closed vortices, with exponentially decaying strengths, interacts with neighbouring Stokeslets. From (4.5) and (4.7) we see that ψ^z is symmetric around $z = \frac{1}{2}\Lambda$, and ψ^R antisymmetric, so only lines in the range $0 \leqslant z \leqslant \frac{1}{2}\Lambda$ need be shown.

Figures 2(*a*) and 3(*a*) show ψ^z and ψ^R for $\kappa = 0.3$ and $b = 0.95$. For $\kappa = 0.3$ we have $\Lambda = 20.944$. Thus all interaction with neighbouring Stokeslets is completely negligible and we obtain essentially the solution due to a single ring of Stokeslets in an infinite pipe. For large Λ, as in this case, we see from (4.5) and (4.7) that unless z is very close to zero, $\psi^z \sim \exp(-\mathrm{Re}\,(d_1)\, z) = \exp(-4.466\, z)$, since the second term in the series is only a few percent of the first term already at $z = 1.0$. Thus the solution is exponentially decreasing, and ψ is shown only up to about $z = 4.0$. Breaking up into disjoint cells is seen in all cases. Both ψ^z and ψ^R are similar in appearance, except near the Stokeslet line $z = 0$, where ψ^z creates a single vortex whereas ψ^R creates a pair of them, $z = 0$ being a streamline. Figures 2(*b*) and 3(*b*) show ψ^z and ψ^R for $\kappa = 3.0$ ($\Lambda = 2.0944$). The distance is still over twice the radius, but some interaction may be expected.

Figure 2(*b*) shows that interaction has not yet taken place. For values of b closer to the axis the retarding effect of the wall is less dominant and some interaction does take place. An example is shown in figure 4, where a complete wavelength is shown. Figure 3(*b*) shows ψ^R. Because $z = \frac{1}{2}\Lambda$ is always an antisymmetry line we have separated cells of flow, and the cells are 'squeezed' into the width of $\frac{1}{2}\Lambda$.

Figures 2(*c*) and 3(*c*) show streamlines for $\kappa = 30.0$ ($\Lambda = 0.20944$). Here we have five Stokeslets per unit length downstream, and we expect strong interaction. The z-dependence of ψ^z, as seen in (4.2), is in the two infinite series. The first has terms which decay exponentially like $\exp[-\kappa m|b-R|]$, and the second has terms decaying exponentially like $\exp\{-\kappa m[(1-R)+(1-b)]\}$. If $|b-R|$ is not too small both series are small compared with $f(R, b)$ in (4.2), and we expect streamlines parallel to the z-axis. Indeed that is what we obtain in figure 2(*c*), with the fluid moving downstream near the walls and upstream near the axis. For smaller values of b, directions are reversed, but the same phenomenon is seen. Notice that even at $b = 0.95$ a density of five Stokeslets per unit length is sufficient to completely annihilate the vortices and create a continuous non-separated flow. Equation (4.7) shows very little variation

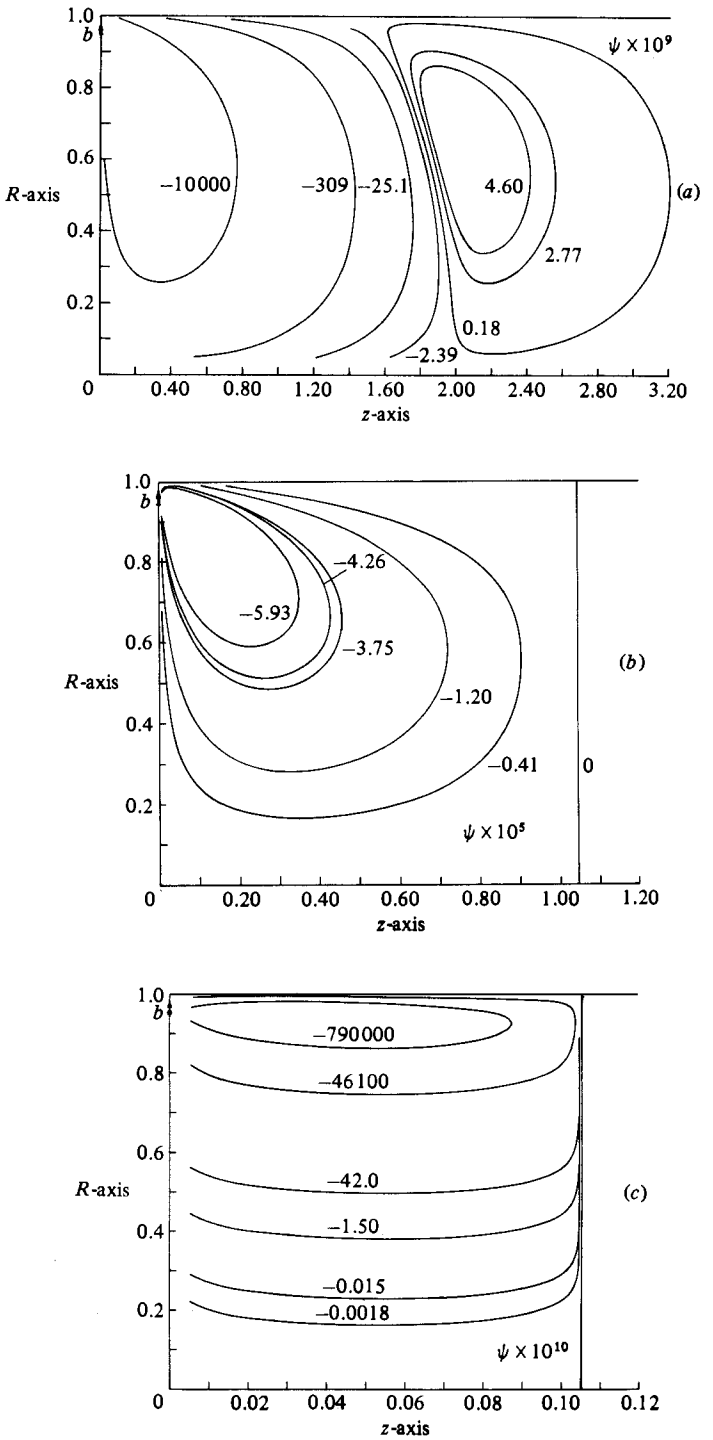

FIGURE 3. Streamlines for Stokeslets in the radial direction (see (4.6) and (4.7)) situated at a radius $b = 0.95R_0$, for: (*a*) $\kappa = 0.3$; (*b*) 3; (*c*) 30. The flow field is antisymmetric around $z = 0$ and $z = \frac{1}{2}\Lambda$, and only the range $0 < z < \frac{1}{2}\Lambda$ is shown.

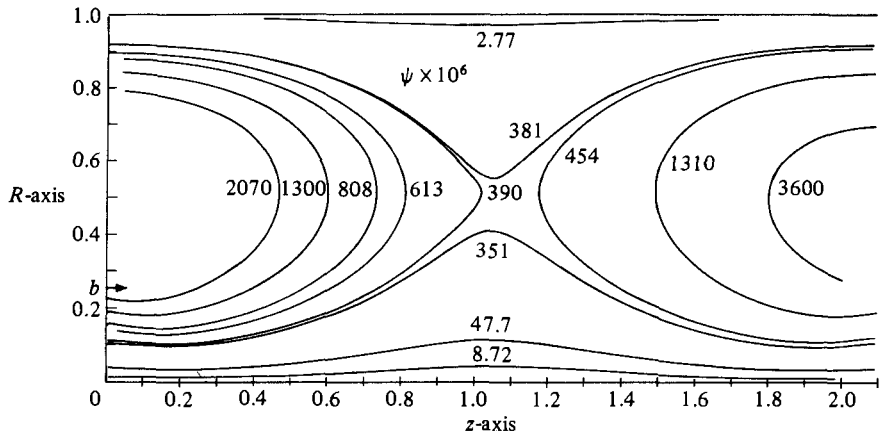

FIGURE 4. Streamlines for Stokeslets in the z-direction (see (4.2) and (4.5)) situated at a radius $b = 0.25R_0$ for $\kappa = 3.0$. $\kappa = 2\pi/\Lambda$ is the wavenumber of the Stokeslets. A full period $0 < z < \Lambda$ is shown, and interaction is seen causing a continuous stream near the centre of the pipe and near the pipe wall.

of ψ^R in z for $0 < z < \frac{1}{2}\Lambda$, and from (4.6) $\psi^R = 0$ at $z = 0, \frac{1}{2}\Lambda$. Thus we obtain the streamlines obtained in figure 3*c*. The flow created enhances a parallel flow (parallel to axis) even in this case where the Stokeslets are directed radially, except very near the antisymmetry lines $z = 0$ and $z = \frac{1}{2}\Lambda$.

5. Integral equations for the force distribution

To obtain the force coefficients, we fit kinematically to the observed cilia beat as has been done in Liron & Mochon (1976*a*) and Liron (1978):

$$\frac{\partial \xi_j^n}{\partial t}(\bar{s},t) = U_j(\xi_1^n(\bar{s},t),\ na+\xi_2^n(\bar{s},t),t)$$

$$= v_j(\xi_1^n(\bar{s},t)) + N\sum_{l=0}^{m_0-1}\int_0^1 F_\kappa(\xi^l(s,t))\,D_j^k(\xi_1^n(\bar{s},t),\xi_2^n(\bar{s},t)+(n-l)\,a,\xi^l(s,t))\,\mathrm{d}s$$

$$(n = 0,1,\ldots,m_0-1, j = 1,2), \quad (5.1)$$

where ξ^l is defined in (2.17). The Poiseuille flow v_j is determined by first solving the extreme case:

(i) $Q = 0, \Delta P = \Delta P^{\max}$, for which $v_j = 0$ in (5.1).

Equations (3.1) can be solved and then $\Delta P^{\max}$ computed from (2.22).

(ii) Take any $Q > 0$; then from (2.23) one obtains the pressure gradient for the Poiseuille flow, computes v_j from (2.19), and then solves (5.1). ΔP is computed from (2.22) to check that $\Delta P \geqslant 0$, and we are in the pumping range. In practice, the Poiseuille-flow contribution in the cilia layer is small compared to the cilia velocities. This implies that the forces change very little by adding v_j, and one can obtain the flow with $\Delta P = 0$ and $Q = Q^{\max}$, by substituting

$$-\frac{\partial P}{\partial z} = \frac{\Delta P^{\max}}{\lambda}$$

in (2.19) for v_j, and then solving (5.1).

Then, combining (5.1), (2.22) and (2.19), we obtain

$$\frac{\partial \xi_j^n(\bar{s},t)}{\partial t} = N \sum_{l=0}^{m_0-1} \int_0^1 F_k(\xi^l(s,t))\, D_j^k(\xi_1^n(\bar{s},t), \xi_2^n(\bar{s},t) + (n-l)\,a, \xi^l(s,t))\,\mathrm{d}s$$
$$+ \alpha\delta_{j2} \frac{R_0^2 - \xi_1^n(\bar{s},t)^2}{4\mu} N \sum_{l=0}^{m_0-1} \int_0^1 F_2(\xi^l(s,t)) \frac{\kappa}{\pi^2 R_0^2}\left[1 - \left(\frac{\xi_1^l(s,t)}{R_0^2}\right)^2\right]\mathrm{d}s$$
$$(n = 0, \ldots, m_0 - 1, j = 1, 2), \quad (5.2)$$

where $\alpha = 0$ for $Q = 0$ and $\Delta P^{\max}$, and $\alpha = 1$ for $Q^{\max}$ and $\Delta P = 0$.

The equations are non-dimensionalized by using the timescale σ^{-1}, lengthscale R_0, velocity scale σR_0, force scale $\mu\sigma R_0^2$ and pressure scale $\mu\sigma$. Redefining $(\kappa N/4\pi^2)\boldsymbol{F}$ as $\boldsymbol{F}$ and $(4\pi^2/\kappa)\, D_j^k$ as D_j^k, (5.2) in non-dimensional form becomes

$$\frac{\partial \xi_j^n(\bar{s},t)}{\partial t} = \sum_{l=0}^{m_0-1} \int_0^1 \{F_k(\xi^l(s,t))\, D_j^k(\xi_1^n(\bar{s},t), \xi_2^n(\bar{s},t) + (n-l)\,a, \xi^l(s,t))$$
$$+ \delta_{j2}\,\alpha(1 - \xi_1^n(\bar{s},t)^2)\, F_2(\xi^l(s,t))\,(1 - \xi_1^l(s,t)^2)\}\,\mathrm{d}s$$
$$(n = 0, 1, 2, \ldots, m_0 - 1, j = 1, 2). \quad (5.3)$$

Equation (5.3) causes no problem, except when $s = \bar{s}$ and $l = n$. D_j^k then becomes singular. In Liron (1978) this was overcome by replacing the action of the Stokeslet on itself, by a point at the same cross-section on the cilium surface. This was not satisfactory, since without an adjoining Doublet distribution it depended on the location on the surface, even on the same cross section. Lighthill (1976) has demonstrated that if we distribute Stokeslets and doublets in an appropriate way on the centreline of a flagellum then each cross-section element will move locally with a velocity approximately equal to $(1/4\pi\mu)\,\boldsymbol{F}_n + \boldsymbol{f}$, where $\boldsymbol{F}_n$ is the component of force in the normal direction. $\boldsymbol{f}$ is the contribution coming from the distribution of Stokeslets along the centreline a distance $ae^{\frac{1}{2}}$ from the point of observation and on, the flagellum radius and a is. The error incurred is $O(\epsilon)$, where ϵ is the slenderness ratio. Using this idea, we would like to replace D_j^k in (5.3) when $s = \bar{s}$ and $l = n$ by an equivalent expression. D_j^k is the axisymmetric part of an infinite sequence of Stokeslets, or the solution due to an infinite sequence of Stokeslet rings.

Velocities due to $\boldsymbol{F}_n$ are

$$\left.\begin{aligned} S_1^1 &= \frac{1}{4\pi\mu}\cos^2\theta, \quad S_2^2 = \frac{1}{4\pi\mu}\sin^2\theta, \\ S_1^2 &= S_2^1 = \frac{1}{4\pi\mu}\sin\theta\cos\theta, \end{aligned}\right\} \quad (5.4)$$

where θ is the angle between the cilia direction and the pipe surface (see figure 5). The contribution due to $\boldsymbol{f}$ at the point $R = b$, $z = 0$ is

$$\lim_{\substack{R\to b \\ z\to 0}} [D_j^k(R,z,b,0) - \text{single Stokeslet in } \infty \text{ medium at } R = b, z = 0].$$

Thus in $\boldsymbol{f}$ we take into account all other parts of D_j^k: the rest of the Stokeslet ring, all images of the entire ring, and all other rings. This computation cannot be done directly. We first subtract the entire ring plus image contribution, then add ring image, then add the contribution of the rest of the ring to the point of observation (averaged over one Φ-period of $2\pi/N$).

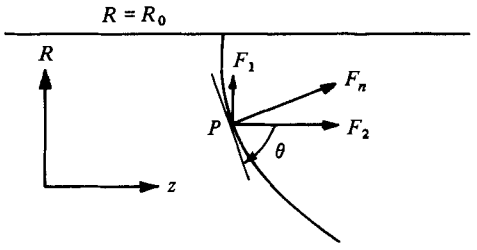

FIGURE 5. Geometry for a cilium movement. Slender body implies that the point P moves in the direction of the normal with velocity $F_n/4\pi\mu$, plus velocities due to the effect of cilium parts further from P (see §5).

The final result is as follows. In (5.3), whenever we are to compute $D_j^k(b,z,b,z)$, we replace it by $\hat{D}_j^k(b)$, where

$$\hat{D}_R^z = \hat{D}_z^R = \frac{\pi}{\kappa N}\sin\theta\cos\theta, \tag{5.5}$$

$$\hat{D}_z^z = \frac{\pi}{\kappa N}\sin^2\theta + \frac{1}{2\kappa b}\ln\cot\frac{\pi}{4N} + \tilde{D}_z^z, \tag{5.6}$$

$$\hat{D}_R^R = \frac{\pi}{\kappa N}\cos^2\theta + \frac{1}{2\kappa b}\ln\cot\frac{\pi}{4N} - \frac{3}{2\kappa b}\cos\frac{\pi}{2N} + \tilde{D}_R^R. \tag{5.7}$$

For θ see figure 5. $\tilde{D}_z^z$ and $\tilde{D}_R^R$ are given by

$$\tilde{D}_z^z = \frac{2\pi}{\kappa}\operatorname{Re}\sum_{n=1}^{\infty}\frac{d_n\,\mathrm{e}^{-d_n a}}{1-\mathrm{e}^{-d_n a}}\left[\frac{B_1(b)}{J_0(d_n)J_1(d_n)}\right]^2 + \frac{1}{\kappa}\int_0^\infty \frac{G_1(b,\lambda)\,\mathrm{d}\lambda}{\Delta(\lambda)} \tag{5.8}$$

and

$$\tilde{D}_R^R = -\frac{2\pi}{\kappa}\operatorname{Re}\sum_{n=1}^{\infty}\frac{d_n\,\mathrm{e}^{-ad_n}}{1-\mathrm{e}^{-ad_n}}\left[\frac{B_2(b)}{J_1^2(d_n)}\right]^2 + \frac{1}{\kappa}\int_0^\infty \frac{G_2(b,\lambda)\,\mathrm{d}\lambda}{\Delta(\lambda)}. \tag{5.9}$$

Here

$$\left.\begin{aligned} G_1(b,\lambda) &= I_0^2(\lambda b) + b^2 I_1^2(\lambda b) - 2I_0(\lambda b)\,[I_0(\lambda b) + \lambda b I_1(\lambda b)]\,A(\lambda), \\ G_2(b,\lambda) &= b^2 I_0^2(\lambda b) + I_1^2(\lambda b) + 2I_1(\lambda b)\,[I_1(\lambda b) - \lambda b I_0(\lambda b)]\left[A(\lambda) + \frac{2}{\lambda^2}\right], \end{aligned}\right\} \tag{5.10}$$

$A(\lambda)$ is defined in (3.5), $\Delta(\lambda)$ in (3.12), B_1 in (3.30), B_2 in (3.36) and d_n in (3.31), and (3.32).

In summary we solve (5.3), which are non-singular, by replacing D_j^k by $\hat{D}_j^k$ whenever D_j^k is singular.

6. Numerical results

6.1. *Description of moving cilium and solution of integral equations*

We use here the same beat as was used in Liron & Mochon (1976) and Liron (1978). The beat is depicted in figure 6, where increasing numbers indicate cilia positions at consecutive fixed time intervals. The description of the moving cilium is achieved in a manner similar to that in the above mentioned papers. We discretize the cilium,

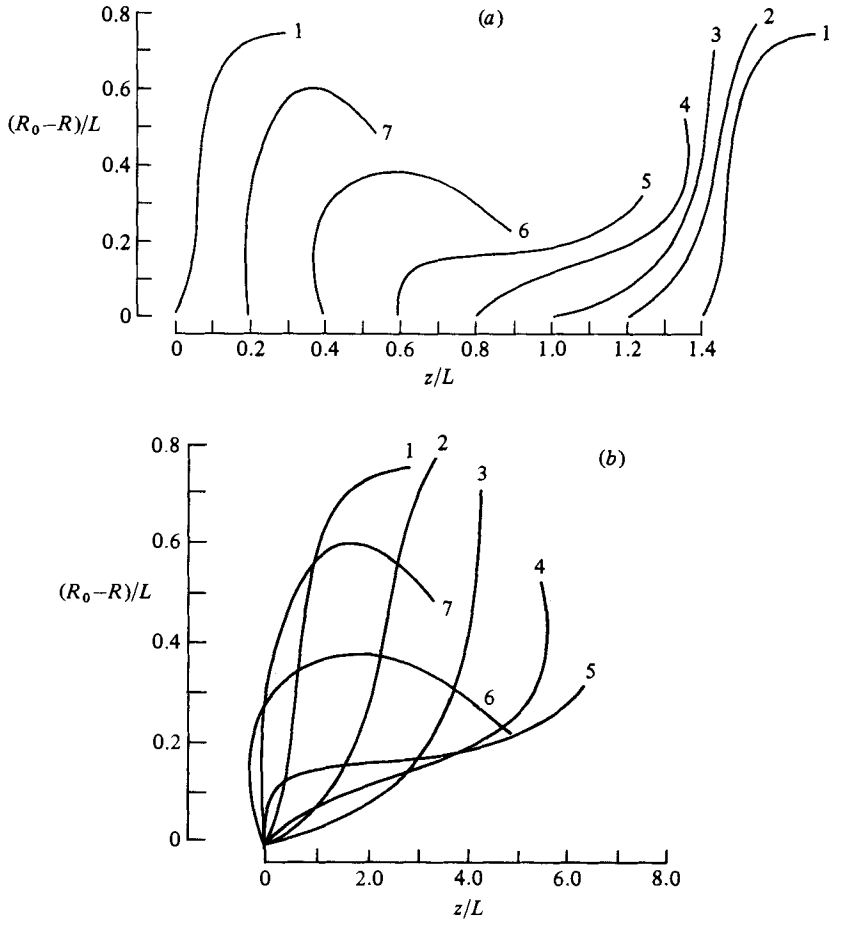

FIGURE 6. The model for cilia beat. (*a*) Cilia positions in one wavelength $\lambda = 1.4L$, with $L \equiv$ cilium length. (*b*) Cilium positions in time. Cilia are assumed to go through the same beat, with a phase difference down the pipe. Increasing numbers indicate consecutive fixed time intervals.

taking M_1 intervals, the mid-points $s_k = (k-\frac{1}{2})/M_1$ $(k = 1, 2m \ldots, M_1)$ representing the intervals. For a fixed s_k we fit its periodic movement by a Fourier-series expansion

$$\xi_i(s_k, t) = \tfrac{1}{2}a_{0i}(s_k) + \sum_{n=1}^{M_2} [a_{ni}(s_k)\cos nt + b_{ni}(s_k)\sin nt]. \tag{6.1}$$

This we differentiate to obtain the cilium velocities. In our calculations we took $M_1 = 7$, $M_2 = 3$. (A check on the accuracy of velocity profiles as a function of M_1, the number of intervals taken along a cilium show $M_1 = 7$ to be sufficient with only small changes for larger values.) The coefficients in (6.1) are found by matching at discrete times $t_l = 2\pi l/(2M_2 + 1)$ $(l = 0, \ldots, 2M_2)$. Equation (5.3) is then discretized by taking the discrete points s_k and t_l. The integration is done using the midpoint rule. Since we are looking at a two-dimensional (R, z) flow we have two components of force, and altogether $2M_0M_1$ linear equations and unknowns. In (5.5)–(5.7) we also have the number N of cilia on the circumference of a cross-section. Assuming that cilia are spaced 1 μm apart in the Φ-direction, $N = 2\pi R_0$, where R_0 is measured in μm.

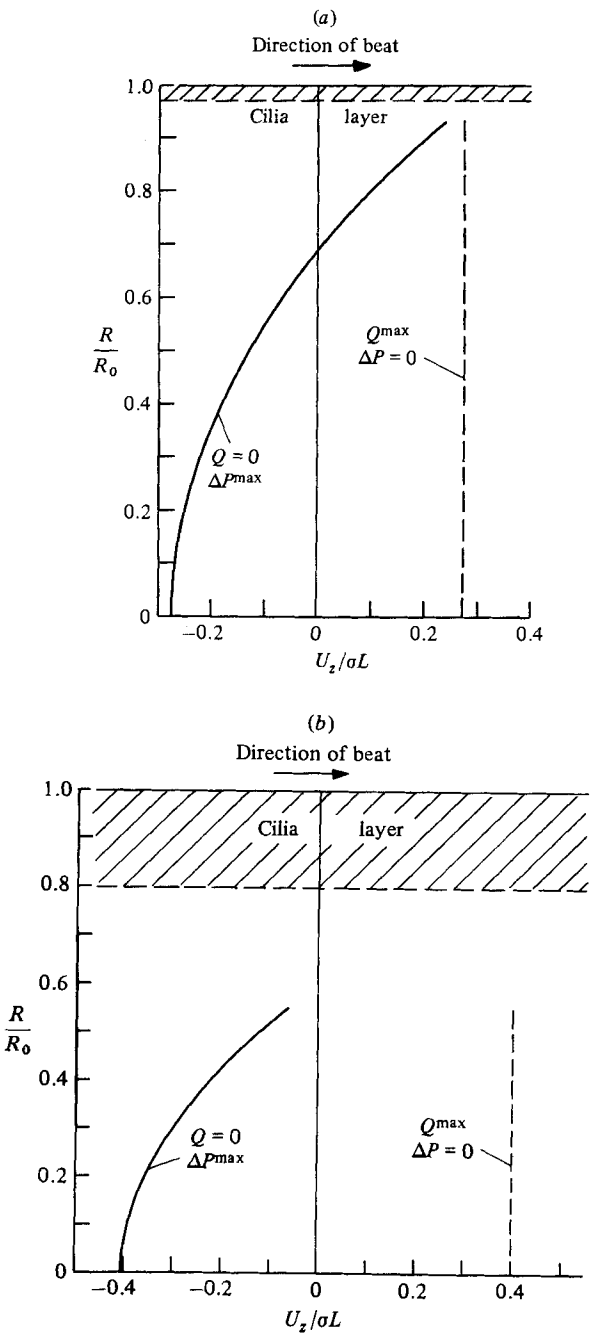

FIGURE 7. Velocity profiles inside the pipe core. Only the downstream velocity exists, and is a function of R only (independent of time and of z). The two extreme cases in the pumping range are exhibited: $Q = 0$, $\Delta P^{\max}$, and $Q^{\max}$, $\Delta P = 0$. All other profiles are parabolas in between. (*a*) $R_0 = 500$ μm, $L = 0.03\ R_0$. (*b*) $R_0 = 75$ μm, $L = 0.2R_0$. Closer to the cilia layer the velocity shows (z, t)-dependence.

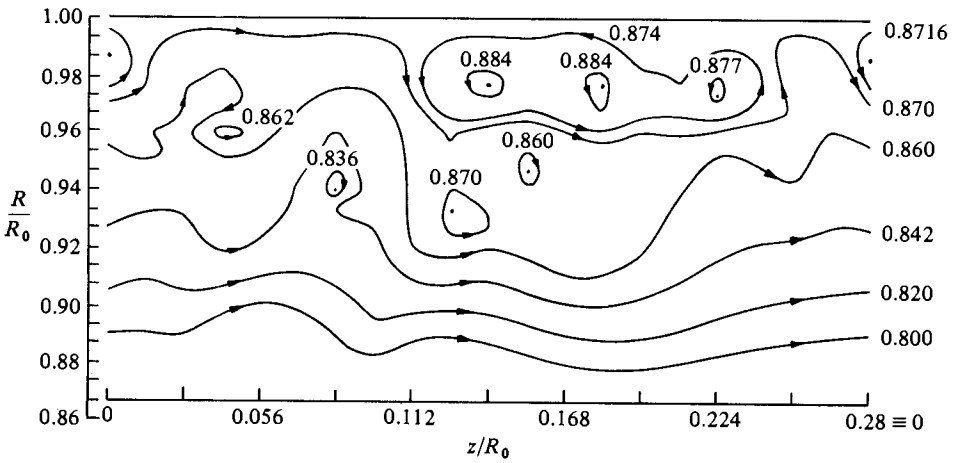

FIGURE 8. Streamline pattern in the ciliary sublayer for the time corresponding to the cilia configuration in figure 6(*a*). $z = 0$ corresponds to cilia base no. 1. Here $R_0 = 75$ μm, $\alpha = 1$ corresponding to $\Delta P = 0$, see also figure 7(*b*).

This is the value we took in the numerical examples below. The calculation of D_j^k is discussed in §3.

Calculation of the infinite series for $\tilde{D}_R^R$ and $\tilde{D}_z^z$ causes no problems, and so is the computation of the infinite integrals, unless b is extremely close to 1.

6.2. *Velocity profiles*

We demonstrate the results by calculating the two extreme cases

$$\alpha = 0 (Q = 0, \Delta P^{\max}), \quad \text{and} \quad \alpha = 1 (\Delta P = 0, Q^{\max}).$$

In figure 7 we present two examples of the flow inside the pipe, and outside the cilia layer. Similar to the results obtained for transport between parallel plates the time (or z) variations die out at about 2 ciliary lengths away from the layer, and we obtain a parabolic profile in the core region which is in the direction opposite to the beat when the flux is zero. The addition of a Poiseuille flow such that altogether $\Delta P = 0$ results in a plug flow which is stronger for a larger ratio of length of cilium to radius. In figure 7(*a*) we show the case of $L = 15\,\mu$m, $R_0 = 500\,\mu$m and (*b*) $L = 15\,\mu$m, $R_0 = 75\,\mu$m.

6.3. *The cilia sublayer*

As we are now solving (5.3) with the corrections (5.5)–(5.7) and the equations are non-singular, we can more reliably than before look at the flow inside the cilia sublayer. To do this, since we have (at every time instant)

$$U_j(R, z, t) = \sum_{l=0}^{m_0-1} \int_0^1 [F_k(\xi^l(s,t))\, D_j^k(R, z - la, \xi^l(s,t)) + \alpha \delta_{j2}(1 - R^2)\, F_2(\xi^l(s,t))\,(1 - \xi^l(s,t)^2)]\, \mathrm{d}s, \quad (6.2)$$

we can define a stream function ψ such that

$$u_1 = u_R = -\frac{1}{R}\frac{\partial \psi}{\partial z}, \quad u_2 = u_z = \frac{1}{R}\frac{\partial \psi}{\partial R}, \quad (6.3)$$

and obtain

$$\psi(R,z,t) = \sum_{l=1}^{m_0-1} \int_0^1 [F_k(\xi^l(s,t))\,\psi^k(R, z-la, \xi^l(s,t)) + \alpha(\tfrac{1}{2}R^2 - \tfrac{1}{4}R^4)\,F_2(\xi^l(s,t))\,(1-\xi_1^l(s,t)^2)]\,\mathrm{d}s. \quad (6.4)$$

The functions ψ^k ($k = 1, 2$) are given in (4.6) and (4.2) respectively.

In figure 8 we show streamlines at time t corresponding to the cilia configuration in figure 5, with $z = 0$ at the base of cilium no. 1, for the case $R_0 = 75$, $\alpha = 1$. Inside the cilia layer, close to the base there are closed vortices and counter-currents, but already towards the end of layer the flow becomes unidirectional with variations which are rather small. As mentioned above, at about two cilia lengths the flow becomes completely uniform.

7. Discussion

We have presented here a model of cilia fluid transport in a pipe. The cilia are modelled by the discrete-cilia approach using the singularity method and slender-body theory. As expected from previous work on cilia transport between parallel plates, although velocities change inside the ciliary layer, time variations die out as we move away from the layer and the flow becomes time-independent, and varies from a backward parabolic profile to a forward plug flow, in the pipe core, (depending on flux conditions) in the pumping range. The problem of solving numerically the singular equation for the force-coefficients has now been satisfactorily overcome as explained in §5.

The basic building block in the model is the Green function D_j^k (see (2.18)). This is the flow field due to an infinite series of Stokeslets and is discussed extensively in §§3 and 4. This function is used in (6.2) to compute the velocity field. Since the single Stokeslet field decays exponentially away from the force's point of action, the parabolic field obtained is practically a local result, due to the near field, the cilia as of a few radii away contributing exponentially small corrections to it. It follows that given the flux (or pressure rise per wavelength) the parabolic profile would obtain provided we have a straight stretch of a few radii length. Convoluting the pipe would thus not change the result, and we would expect to observe the same local profile along the tube. Thus although the model is for an infinite straight pipe, the results are applicable to a convoluted pipe like the oviduct. As already explained in Liron (1978), the case $Q = 0$ might be realistic during ovulation, when the Ampulla–isthmus junction is completely or almost completely occluded. The back flow in the pipe core might be responsible for the ability of sperm to be moved up the oviduct from the uterus to the site of fertilization, even though cilia beat is directed towards the uterus. As observed by Blandau (1969) spermatozoa were observed to be swept along by the ciliary current when applied to the surfaces of opened oviducts at such a rate that their own flagellar activity was of almost no avail against the current.

Streamlines in the cilia layer show a directional flow in the upper part of the layer but vortices in the lower part. This may explain observations claiming backflow near the cilia bases. Obviously, the vortices here are only an example, for the given beat used, but they show that even here the complicated pattern blends nicely into the parallel flow further away from the wall.

The examination of the Green function D_j^k shows that already at a distance of $0.2R_0$ between Stokeslet rings the flow created has practically a single velocity component

(downstream) which has a parabolic profile (Poiseuille plus shear flow). Thus the flow field created by cilia which are densely packed on the surface of the pipe is a continuous flow as described above. The same flow would be created by a cluster of small beads, sedimenting in a pipe, as in the Segré & Silberberg (1962) results.

REFERENCES

ABRAMOWITZ, M. A. & STEGUN, I. A. 1965 *Handbook of Mathematical Functions*. Dover.

BLAKE, J. R. 1972 A model for the micro-structure in ciliated organisms. *J. Fluid Mech.* **55**, 1–23.

BLAKE, J. R. 1973 Flow in tubules due to ciliary activity. *Bull. Math. Biol.* **35**, 513–523.

BLAKE, J. R. 1979 On the generation of viscous toroidal eddies in a cylinder. *J. Fluid Mech.* **95**, 209–222.

BLAKE, J. R., LIRON, N. & ALDIS, G. K. 1982 Flow patterns around ciliated microorganisms and in ciliated ducts. *J. Theor. Biol.* **98**, 127–141.

BLANDAU, R. J. 1969 Gamete transport-comparative aspects. In *The Mammalian Oviduct* (ed. E. S. E. Hafez & R. J. Blandau). University of Chicago Press.

BLUM, J. J. 1974 A note on fluid transport in ciliated tubules. *J. Theor. Biol.* **46**, 287–290.

FRIEDMANN, M., GILLIS, J. & LIRON, N. 1968 Laminar flow in a pipe at low and moderate Reynolds numbers. *Appl. Sci. Res.* **19**, 426–438.

HASIMOTO, H. & SANO, O. 1980 Stokeslets and eddies in creeping flows. *Ann. Rev. Fluid Mech.* **12**, 335–363.

LARDNER, T. J. & SHACK, W. J. 1972 Cilia transport. *Bull. Math. Biophys.* **34**, 325–335.

LIGHTHILL, M. J. 1976 Flagellar Hydrodynamics – The John von Neumann Lecture, 1975. *SIAM Rev.* **18**, 161–230.

LIRON, N. 1978 Fluid transport by cilia between parallel plates. *J. Fluid Mech.* **86**, 705–726.

LIRON, N. & BLAKE, J. R. 1981 Existence of viscous eddies near boundaries. *J. Fluid Mech.* **107**, 109–129.

LIRON, N. & MEYER, F. A. 1980 Fluid transport in a thick layer above an active ciliated surface. *Biophys. J.* **30**, 463–472.

LIRON, N. & MOCHON, S. 1976*a* The discrete cilia approach to propulsion of ciliated micro-organisms. *J. Fluid Mech.* **75**, 593–607.

LIRON, N. & MOCHON, S. 1976*b* Stokes flow for a Stokeslet between two parallel flat plates. *J. Engng Maths* **10**, 287–303.

LIRON, N. & SHAHAR, R. 1978 Stokes flow due to a Stokeslet in a pipe. *J. Fluid Mech.* **86**, 727–744.

MOFFATT, H. K. 1964 Viscous and resistive eddies near a sharp corner. *J. Fluid Mech.* **18**, 1–18.

SEGRÉ, G. & SILBERBERG, A. 1962 Behaviour of macroscopic rigid spheres in Poiseuille flow. Part 2. Experimental results and interpretation. *J. Fluid Mech.* **14**, 137–157.